crystals

Article

Acoustic Tunneling Study for Hexachiral Phononic Crystals Based on Dirac-Cone Dispersion Properties

Luyun Chen [1], Yong Liu [2] and Hui Kong [1,*]

[1] MOE Key Lab Marine Intelligent Equipment & System, Shanghai Jiao Tong University, Shanghai 200240, China; cluyun@sjtu.edu.cn
[2] China Ship Scientific Research Center, Shanghai Branch, Shanghai 200011, China; clyhn@sohu.com
* Correspondence: linda2018@sjtu.edu.cn; Tel.: +86-021-3420-7165

Abstract: Acoustic tunneling is an essential property for phononic crystals in a Dirac-cone state. By analyzing the linear dispersion relations for the accidental degeneracy of Bloch eigenstates, the influence of geometric parameters on opening the Dirac-cone state and the directional band gaps' widths are investigated. For two-dimensional hexachiral phononic crystals, for example, the four-fold accidental degenerate Dirac point emerges at the center of the irreducible Brillouin zone (IBZ). The Dirac cone properties and the band structure inversion problem are discussed. Finally, to verify acoustic transmission properties near the double-Dirac-cone frequency region, the numerical calculation of the finite-width phononic crystal structure is carried out, and the acoustic transmission tunneling effect is proved. The results enrich and expand the manipulating method in the topological insulator problem for hexachiral phononic crystals.

Keywords: phononic crystal; band structure; Dirac-cone dispersions; acoustic tunneling

Citation: Chen, L.; Liu, Y.; Kong, H. Acoustic Tunneling Study for Hexachiral Phononic Crystals Based on Dirac-Cone Dispersion Properties. *Crystals* **2021**, *11*, 1577. https://doi.org/10.3390/cryst11121577

Academic Editors: Luis M. Garcia-Raffi and Víctor J. Sánchez-Morcillo

Received: 30 November 2021
Accepted: 15 December 2021
Published: 17 December 2021

1. Introduction

Acoustic/elastic wave control and acoustic transmission suppression by using phononic crystals has become a research hotspot in recent years [1–3]. Theoretical analysis, numerical calculation, and experiments were conducted to analyze acoustic waveguiding, acoustic collimating, acoustic focusing, acoustic negative refraction, unidirectional transmission, seismic prevention, acoustic wave filtering, localization, and so on [4–7]. The band structure properties, named band gaps, are the key index to evaluate the mechanical performance of phononic crystals. The width and position of the band gaps are highly dependent on the geometric parameters and material parameters of the phononic crystal cell [8].

In the band structure, two or more energy bands intersect linearly at one point, named a Dirac point, on the boundary of the irreducible Brillouin zone of the phononic crystal [9–11]. Dirac points have three forms, namely, the double Dirac cone, single Dirac cone, and Dirac-like cone [12,13]. Among them, the double Dirac cone is formed by an inverted pair of two identical Dirac cones [14,15]. Strange physical phenomena that exist at the Dirac point include pseudodiffusion transmission, edge states, quavers, acoustic topological insulators, acoustic tunneling, and so on [16,17]. By adjusting the geometric parameters, the Dirac cones are broken and new directional band gaps are formed [18,19]. Some special acoustic properties appeared at the double Dirac cone, which have an important influence on the application of phononic crystals [20,21]. Recently, the massless relativistic dispersion problem in Dirac cones has become the focus in acoustic metamaterials, including the acoustic wave tunneling problem [22,23].

In the hexachiral phononic crystal, the scatterers are connected by six adjacent ligaments [24]. The mechanical performance of the hexachiral phononic crystal is mainly determined by ligament thickness, scatterer diameter, and so on [25,26]. Due to the chirality, the hexachiral phononic crystals do not have complete mirror symmetry, which gives a great influence on acoustic transmission and the acoustic topological insulator [27,28].

However, only a few studies have been conducted on the band structure properties of hexachiral phononic crystals at present; analyses of the Dirac cone problem for hexachiral phononic crystals are still in the exploratory stage.

Based on the reasons mentioned above, the acoustic tunneling problem is studied based on double-Dirac-cone dispersion analysis and band structure inversion analysis for hexachiral phononic crystals. The remainder of the present article is organized as follows: some theories of hexachiral phononic crystals are introduced in Section 2; A four-fold accidental degenerate Dirac point is formed corresponding to special geometric parameters in Section 3; the band structure inversion problem is investigated in Section 4; Acoustic transmission tunneling analysis is implemented numerically in Section 5; finally, some conclusions are summarized in Section 6.

2. Two-Dimensional Hexachiral Phononic Crystal Theory

2.1. Hexachiral Phononic Crystals

Hexachiral phononic crystals are composed of cylindrical scatterers, connection ligaments, and filler matrix. The scatterer is a cylindrical metal body, and six ligaments are attached tangentially onto each scatterer; it is assumed that the ligaments and the cylindrical metal bodies are perfectly bonded, as shown in Figure 1a.

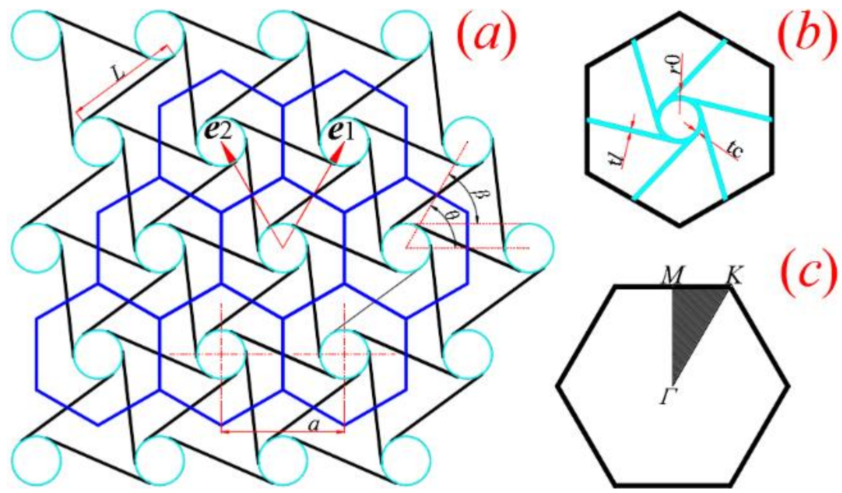

Figure 1. Diagram of the hexachiral phononic crystal schematic: (**a**) Lattice vector, (**b**) Unite cell parameter, and (**c**) Irreducible Brillouin zone.

In Figure 1a, the lattice vectors $\mathbf{e}_1$ and $\mathbf{e}_2$ are used to define the periodicity of the hexachiral phononic crystal. In Figure 1b, the basic design parameters of the hexachiral phononic crystal are as follows: the lattice constant is a, the scatterer radius is r_0, the coating thickness is t_c, and the ligament's thickness is t_l.

2.2. Band Structure of Phononic Crystals

The band structure properties of phononic crystals are the key index to evaluate the insulation performance of the acoustic metamaterials. Defining the wave vector and eigenvalue as horizontal coordinates and longitudinal coordinates, respectively, the band structure curves of a hexachiral phononic crystal are graphed. In the band structure curves, more than one band gap exists within the calculated frequency range. If the complete band gaps are located between the nth and $(n + 1)$th bands, the complete band gap width can be written as:

$$\Delta\omega_n = \min_{\mathrm{k}} : \omega_{n+1}(\mathbf{k}) - \max_{\mathrm{k}} : \omega_n(\mathbf{k}), \tag{1}$$

where $\omega_{n+1}(\mathbf{k})$ is the frequency value of the $(n + 1)$th band, and $\omega_n(\mathbf{k})$ is the frequency value of the nth band. $\min_{\mathrm{k}} : \omega_{n+1}(\mathbf{k})$ and $\max_{\mathrm{k}} : \omega_n(\mathbf{k})$ are the upper and lower bound frequencies, respectively.

3. Dirac Cone of a Hexachiral Phononic Crystals

3.1. Model Description

The band structure problems of 2-D hexachiral phononic crystals are investigated. In the band structure analysis, all finite-element model (FEM) predictions are calculated by using COMSOL Multiphysics software. The FE model of hexachiral phononic crystals is shown in Figure 2.

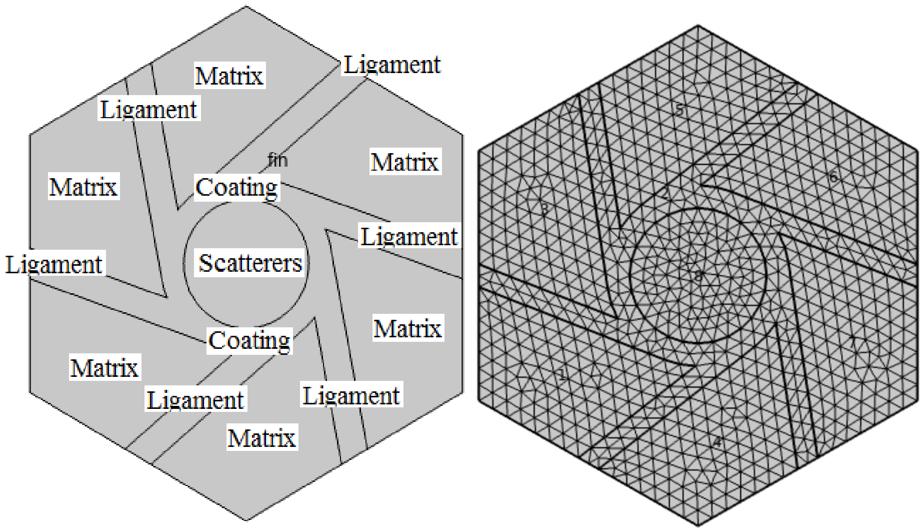

Figure 2. FE model of the 2D hexachiral phononic crystal.

The hexachiral phononic crystal consists of three kinds of materials, namely water, epoxy resin, and steel. The coating of the scatterer and ligament have the same materials. The ligament and coating material are epoxy resin, the matrix material is water, and the scatterer material is steel. The mechanical properties of steel, epoxy resin, and water are shown in Table 1.

Table 1. Material parameters of hexachiral phononic crystal.

Component	Materials Type	Longitudinal Wave Velocities (m/s)	Density (kg/m^3)
Scatterer	steel	5760	7850
Ligament	epoxy resin	2830	1300
Coating	epoxy resin	2830	1300
Matrix	water	1480	1000

3.2. Dirac Cone Point Calculation

In the band structure calculation, the positions of the three high-symmetry points are as follows: $\mathrm{K}(\frac{2\pi}{3a}, \frac{2\sqrt{3}\pi}{3a})$, $\Gamma(0,0)$ and $\mathrm{M}(0, \frac{2\sqrt{3}\pi}{3a})$, as shown in Figure 1c.

The band structure of a phononic crystal can be calculated by sweeping the wave vector $\mathbf{k} = (\mathbf{k}_x, \mathbf{k}_y)$ in the irreducible Brillouin zone (IBZ); the sweeping direction is $K \to \Gamma \to M \to K$, and the band structure curves of the hexachiral phononic crystal are graphed, as shown in Figure 3.

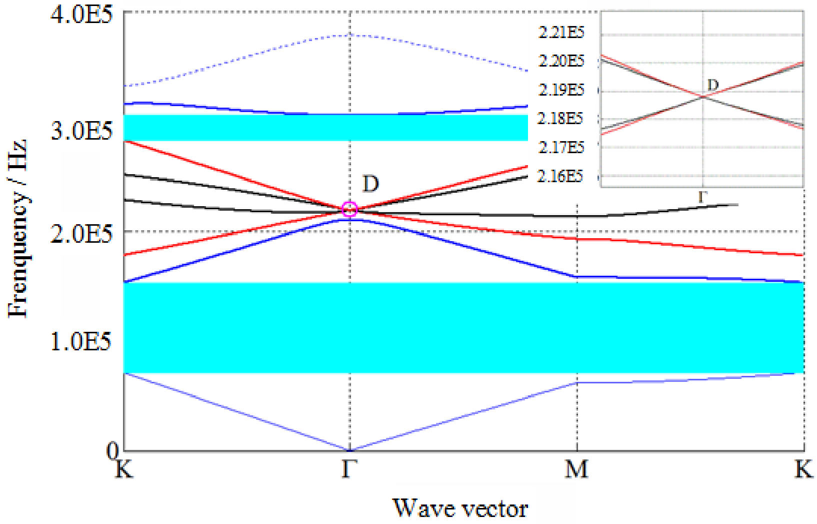

Figure 3. Diagram of band structure for two-dimensional hexachiral phononic crystal (Four-fold degeneracy is appeared at high-symmetry point Γ, the enlarged view around point D is shown in the inset).

There exists an 8-band structure, which contains two complete band gaps shaded with gray. The first band gap is located between the first band and the second band structure, and the second band gap is located between the sixth band and the seventh band structure.

By adjusting the geometric parameters of the hexachiral phononic crystal, a four-fold accidental degenerate double Dirac cone are formed, namely a double-Dirac-cone state. In a double-Dirac-cone state, the geometric parameters of the phononic crystal are as follows: lattice constant a = 8 mm, scatterer diameter r_0 = 1.30 mm, coating thickness $t_c = 0.45$ mm, and ligament thickness $t_l = 0.35$ mm.

According to the band-folding theory, the third, fourth, fifth, and sixth bands of the phononic crystal are closed at the frequency of 218,796.6 Hz, forming four accidental degenerate Dirac points (marked as "D"), as shown in Figure 3. The enlarged view at the top right-hand corner shows the double Dirac cones in the center of the Brillouin zone. The dispersion curve near the Dirac cones point is linear, and the four energy bands are approximately merged into two linear energy bands.

4. Breaking of Double Dirac Cone and Band Inversion

4.1. Band Structure Analysis

Three geometric parameters of the phononic crystal are defined as design-variable (including coating thickness, ligament thickness, and scatterer diameter). If the lattice constants and sweep direction are unchanged, by increasing or decreasing the geometric parameters of the phononic crystal, the dispersion curves between the frequency and the wave vector can be obtained, as shown in Figure 4.

In comparison with Figure 3, the band structure curves of the phononic crystal are altered, and the complete band gaps' width, lower bound frequency and upper bound frequency are varied. In the center of the Brillouin zone, the double-Dirac-cone state is destroyed, the double Dirac-cone state is split into two single Dirac-cone states, marked as "Upper" and "Lower", respectively. In addition, a new directional band gap appears between the fourth and fifth band structures, as shown in the enlarged view at the top right-hand corner. The directional band gap widths for hexachiral phononic crystals are shown in Table 2.

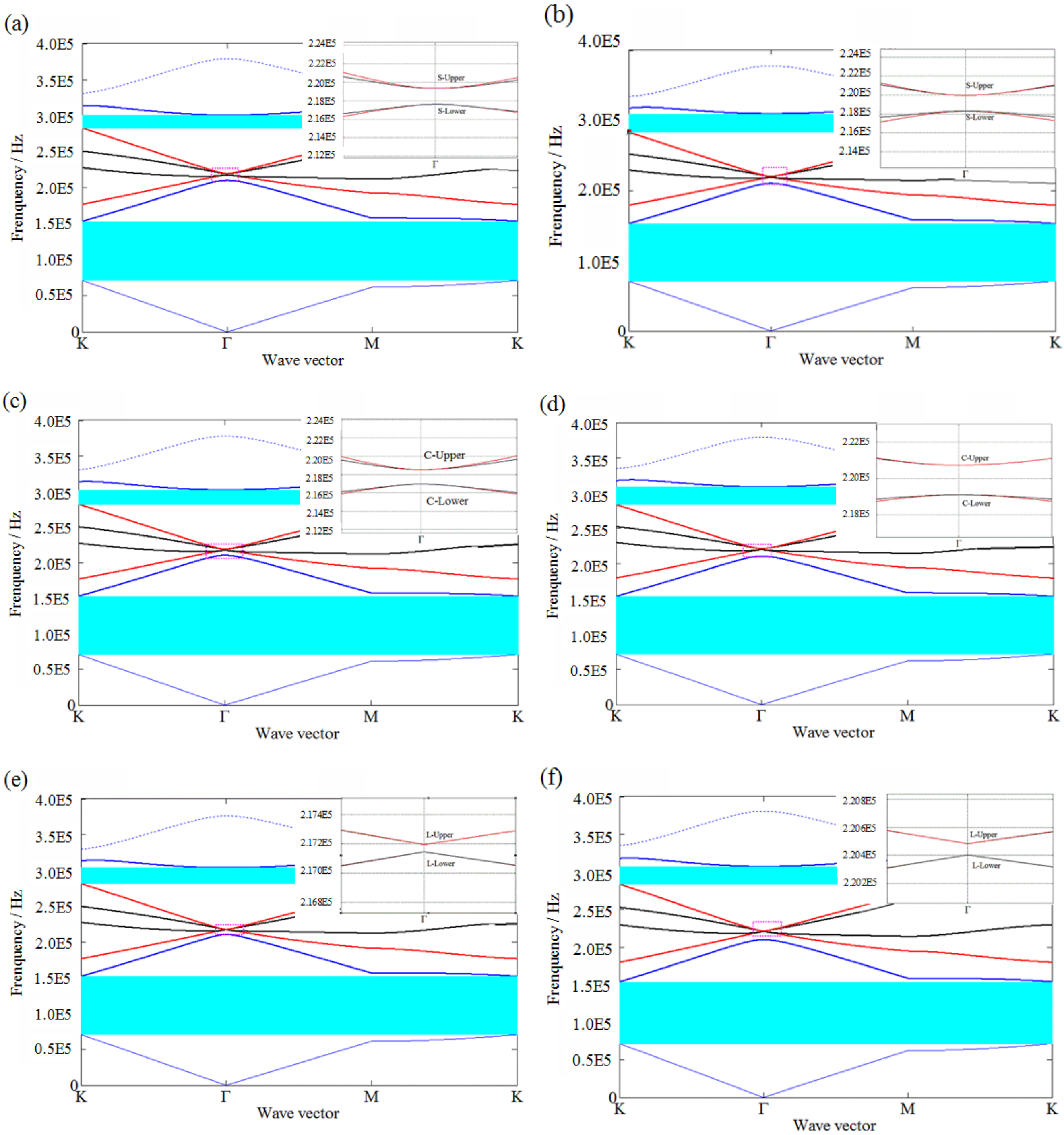

Figure 4. Dispersion curves of hexachiral phononic crystal with different parameters (the inset shows an enlarged view): (**a**) Case A (r_0 = 1.25 mm, t_c = 0.45 mm, and t_1 = 0.35 mm); (**b**) Case B (r_0 = 1.35 mm, t_c = 0.45 mm, and t_1 = 0.35 mm); (**c**) Case C (r_0 = 1.30 mm, t_c = 0.40 mm, and t_1 = 0.35 mm); (**d**) Case D (r_0 = 1.30 mm, t_c = 0.50 mm, and t_1 = 0.35 mm); (**e**) Case E (r_0 = 1.30 mm, t_c = 0.45 mm, and t_1 = 0.30 mm) and (**f**) Case F (r_0 = 1.30 mm, t_c = 0.45 mm, and t_1 = 0.40 mm).

Table 2. Directional band gap width comparison of hexachiral phononic crystals.

Geometric Parameters		Lower Bounds Frequency/Hz	Upper Bounds Frequency/Hz	Directional Band Gap Width/Hz	Band Gap Center Frequency/Hz
Double-Dirac-cone state		218,796.6	218,796.6	0	218,796.6
Scatterer diameter	Case A	217,613.1	219,341.7	1728.6	218,477.4
	Case B	218,317.1	219,969.3	1652.2	219,143.2
Coating thickness	Case C	216,950.9	218,509.7	1558.8	217,730.3
	Case D	219,107.9	220,732.6	1624.7	219,920.2
Ligament thickness	Case E	217,146.3	217,193.8	47.5	217,170.0
	Case F	220,402.3	220,481.7	79.4	220,442

4.2. Band Gap Width Analysis

The influence of geometric parameters on the directional band gap width and the opening of the double Dirac cone are investigated. The relationships among the geometric parameters' deviation of scatterer diameter, ligament thickness, coating thickness, and the directional band gaps' width problem are investigated, as shown in Figure 5. In the numerical analysis, the variation step size of the design variable is 0.01 mm.

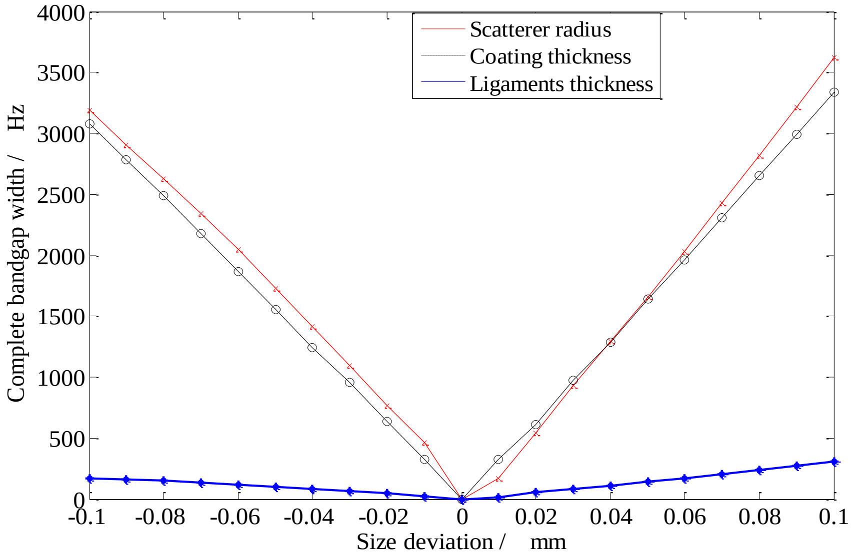

Figure 5. Relationship diagram of design parameter deviation and band gap width frequency.

In Figure 5, in the double-Dirac-cone state, the directional band gap width is 0. By increasing or decreasing the scatterer diameter, ligament thickness, and coating thickness, the band gap width changes approximately linearly, and the ligament thickness is insensitive in contrast to scatterer diameter and coating thickness.

4.3. Band Inversion Analysis

By adjusting the geometric parameters of the hexachiral phononic crystal, the four-fold accidental degenerate Dirac state of the phononic crystal will be destroyed, and the band inversion properties are evaluated. There exist two double-degenerate states in the center of the Brillouin zone. The acoustic pressure distributions of two double-degenerate states in the center of the Brillouin zone are obtained; there are a pair of quadrupolar modes and a pair of dipolar modes, as shown in Figure 6.

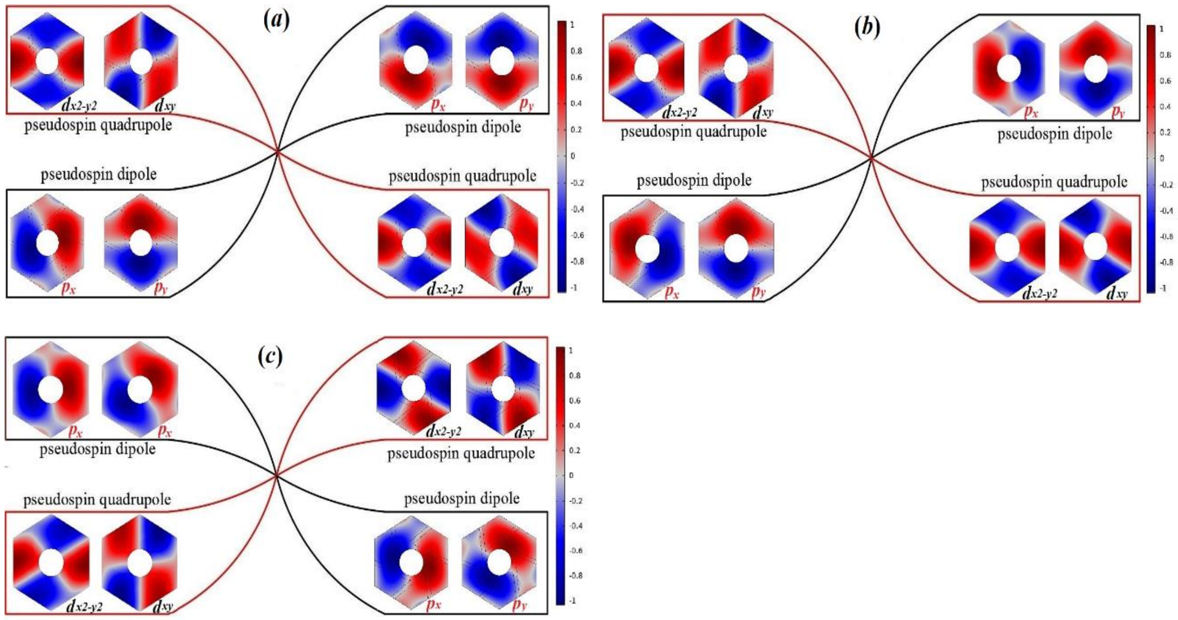

Figure 6. Band inversion process of hexachiral phononic crystal: (**a**) Band inversion process from Case A to Case B; (**b**) Band inversion process from Case C to Case D; and (**c**) Band inversion process from Case E to Case F.

Figure 6 shows acoustic pressure distributions corresponding to the parametric variations of the scatterer diameter, coating thickness, and ligament thickness, respectively. The dark red and dark blue are used to define the positive and negative maxima value. The acoustic pressure field distributions are symmetrical, owing to the properties of the C_{6v} approximate symmetry for the hexachiral phononic crystal cell. The dipole modes are denoted as p_x and p_y, and the quadrupole modes are denoted as d_{xy} and $d_{x^2-y^2}$, respectively. Since the hexachiral phononic crystal is not a perfectly C_{6v}-symmetrical lattice, therefore, they are not perfectly symmetrical to the axes x and y for both dipole modes (p_x and p_y) and quadrupole modes (d_{xy} and $d_{x^2-y^2}$).

In Figure 6a,b, the p-state is in the low-frequency band and the d-state is in the high-frequency band; by increasing the scatterer diameter and coating thickness, the band inversion can transform from a trivial state to a nontrivial state, accompanied by phase transition. In Figure 6c, the d-state is in the low-frequency band and the p-state is in the high-frequency band; by increasing ligament thickness, the band inversion can transform from a trivial state to a nontrivial state accompanied by phase transition.

5. Acoustic Transmission Tunneling Analysis

To demonstrate the band structure properties of phononic crystals, the acoustic transmission calculation for the hexachiral phononic crystal's structure with finite width is necessary. The acoustic transmission phase change and acoustic transmission loss coefficient are compared to analyze the influence of geometric parameters on acoustic transmission performance in the double-Dirac-cone frequency region.

In the acoustic transmission calculation model, the phononic crystal structure consists of hexachiral phononic crystal layers, wave excitation domains, wave evaluation domain, and perfectly matched domains. At the top and bottom edges of the phononic crystal structure, the periodic boundary conditions are implemented. The lengths of the phononic crystal's layer, wave excitation domain, wave evaluation domain, and perfectly matched domain, are 0.10, 0.020, 0.020, and 0.020 m, respectively. The total width of the hexachiral phononic crystal structure is 0.0404 m.

In the numerical calculation, the direction of the incident acoustic wave is perpendicular to the interface between the phononic crystal's layer and the wave excitation domain, and the amplitude value of the incident acoustic wave is 1. The incident acoustic wave frequency is 218796.6 Hz, which corresponds to the double-Dirac-cone frequency.

The loss coefficients for acoustic transmission of the hexachiral phononic crystal structure are shown in Figure 7. The symbol "Scatterer diameter" denotes the geometric parameters corresponding to Case A for Table 2; the symbol "Coating thickness" denotes the geometric parameters corresponding to Case C for Table 2; the symbol "Ligaments thickness" denotes the geometric parameters corresponding to Case E for Table 2; The symbol "Double Dirac cones" denotes the parameter corresponding to the four-fold accidental degenerate Dirac-cone state. The calculated frequency range is 20 to 220 000 Hz, the frequency step size is 2 Hz.

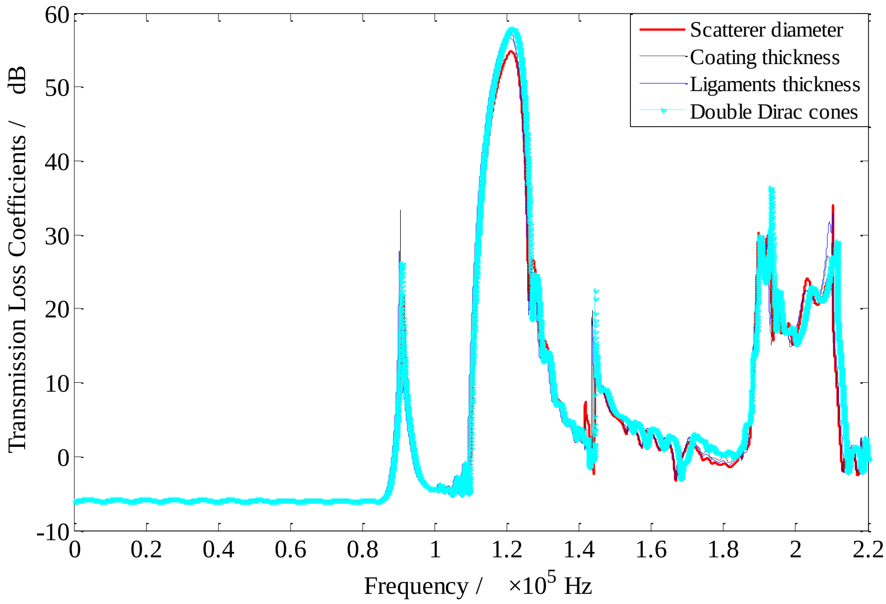

Figure 7. Comparison of loss coefficients for acoustic transmission.

In Figure 7, in the lower frequency band (less than 89,250 Hz), the acoustic transmission loss coefficients are very small. On the other hand, in the double-Dirac-cone frequency region, the acoustic transmission loss coefficients are nearly zero. The results show that the tunneling effect of acoustic transmission appears obviously in the double-Dirac cone-frequency region.

The comparison of acoustic pressure distributions for different geometric parameters of the phononic crystal structure are shown in Figure 8.

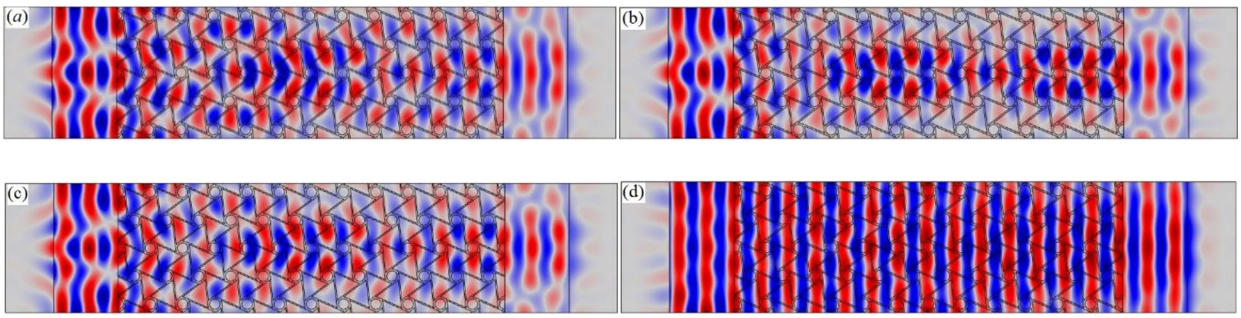

Figure 8. Total acoustic pressure distribution comparison of hexachiral phononic crystals with different geometric parameters: (**a**) (r_0 = 1.25 mm, t_c = 0.45 mm, and t_l = 0.35 mm, corresponds to Case A in Table 2); (**b**) (r_0 = 1.30 mm, t_c = 0.40 mm, and t_l = 0.35 mm, corresponds to Case C in Table 2); (**c**) (r_0 = 1.30 mm, t_c = 0.44 mm, and t_l = 0.30 mm, corresponds to Case E in Table 2); (**d**) (r_0 = 1.30 mm, t_c = 0.45 mm, and t_l = 0.35 mm, corresponds to the four-fold accidental degenerate Dirac cone state).

As shown in Figure 8a–c, substantial phase change occurs inside the phononic crystal structure. On the contrary, the transmission acoustic wave and the incident acoustic wave will be consistent in acoustic pressure amplitude and phase, corresponding to the double-Dirac-point state, as shown in Figure 8d. The tunneling effect at the Dirac point is further verified.

6. Conclusions

The Dirac-cone dispersion properties are systematically investigated for hexachiral phononic crystals in the present article. The influences of design parameters, such as coating thickness, ligament thickness, and cylindrical scatterer diameter on the acoustic topological phase transition are taken into account. The four-fold accidental degenerate Dirac cones of phononic crystals are emerged and disappeared by change the geometric parameters, while the lattice constant is kept unchanged. The band inversion processes occur at the Dirac point. Finally, the Dirac cone properties of hexachiral phononic crystals are unambiguously demonstrated by acoustic transmission calculation, and the tunneling effect is verified. The following conclusions are obtained by numerical analysis: (1) By the introduction of chirality properties, the acoustic transmission manipulation abilities of hexachiral phononic crystals are significantly strengthened; (2) in the double-Dirac-cone frequency region, the relationship between the design parameters and the directional band gaps' width is approximately linear, and the frequency linear dispersion properties are verified; (3) according to the acoustic transmission calculation, an acoustic transmission tunneling effect exists in the double-Dirac-cone frequency; (4) the transmission acoustic wave and the incident acoustic wave will be consistent in acoustic pressure amplitude and phase, corresponding to the double-Dirac-point state, the tunneling effect at the Dirac point is further verified. Some conclusions in this work can provide technical support for the design and application of innovative acoustic metamaterials.

Author Contributions: L.C. put forward the ideas and theoretical model; Y.L. implemented the numerical simulations and data analysis; H.K. revised the manuscript; H.K. and L.C. organized the outline and the whole contents. All authors have read and agreed to the published version of the manuscript.

Funding: This research was funded by the High-tech Ship Research Projects by MIIT.

Institutional Review Board Statement: In this study, without ethical issues involved.

Informed Consent Statement: In this study, without humans involved.

Data Availability Statement: Data is contained within the article.

Conflicts of Interest: On behalf of all authors, the corresponding author states that there are no conflict of interest.

References

1. Saxena, K.K.; Das, R.; Calius, E.P. Three decades of auxetics research-materials with negative Poisson's ratio: A review. *Adv. Eng. Mater.* **2016**, *18*, 1847–1870. [CrossRef]
2. Bolmatov, D.; Zhernenkov, M.; Zav'yalov, D.; Cai, Y.Q.; Cunsolo, A. Terasonic excitations in 2D gold nanoparticle arrays in a water matrix as revealed by atomistic simulations. *J. Phys. Chem. C* **2016**, *120*, 19896–19903. [CrossRef]
3. Bolmatov, D.; Zhernenkov, M.; Sharpnack, L.; Agra-Kooijman, D.M.; Kumar, S.; Suvorov, A.; Pindak, R.; Cai, Y.Q.; Cunsolo, A. Emergent optical phononic modes upon nanoscale mesogenic phase transitions. *Nano Lett.* **2017**, *17*, 3870–3876. [CrossRef]
4. Kaçın, S.; Öztürk, M.; Sevim, U.K.; Özer, Z.; Akgöl, O.; Mert, B.A.; Ünal, E. Experimental verification of phononic crystal based on square arrays of cylindrical holes against seismic vibrations in full-scale systems: Modeling, sensing and signal processing of seismic vibrations. *Arch. Appl. Mech.* **2021**, *112*, 1–15. [CrossRef]
5. Guo, J.J.; Xiao, Y.; Zhang, S.F. Bloch wave based method for dynamic homogenezation and vibration analysis of lattice truss core sandwich structures. *Compos. Struct.* **2019**, *229*, 111437. [CrossRef]
6. Li, S.B.; Chen, T.N.; Wang, X.P.; Li, Y.G.; Chen, W.H. Expansion of lower-frequency locally resonant band gaps using a double-sided stubbed composite phononic crystals plate with composite stubs. *Phys. Lett. A* **2016**, *380*, 2167–2172. [CrossRef]
7. Peng, Y.G.; Qin, C.Z.; Zhao, D.G.; Shen, Y.X.; Xu, X.Y.; Bao, M.; Jia, H.; Zhu, X.F. Experimental demonstration of anomalous Floquet topological insulator for sound. *Nat. Commun.* **2016**, *7*, 13368. [CrossRef] [PubMed]

8. Li, Y.L.; Wang, X.N.; Yan, G.W. Configuration effect and bandgap mechanism of quasi-one-dimensional periodic lattice structure. *Int. J. Mech. Sci.* **2021**, *190*, 106017. [CrossRef]
9. Li, C.; Miao, L.C.; You, Q.; Fang, H.L.; Liang, X.D.; Lei, L.J. Effects of material parameters on the band gaps of two-dimensional three-component phononic crystals. *Appl. Phy. A* **2019**, *106*, 014903. [CrossRef]
10. Wen, X.H.; Qiu, C.Y.; Lu, J.Y.; He, H.L.; Ke, M.Z.; Liu, Z.Y. Acoustic Dirac degeneracy and topological phase transitions realized by rotating scatterers. *J. Appl. Phys.* **2017**, *123*, 091703. [CrossRef]
11. Xia, B.Z.; Wang, G.B.; Zheng, S.J. Robust edge states of planar phononic crystals beyond high-symmetry points of brillouin zones. *J. Mech. Phys. Solids* **2019**, *124*, 471–488. [CrossRef]
12. Pei, D.L.; Yang, T.; Chen, M.; Jiang, H. Underwater acoustic metamaterial based on double Dirac cone characteristics in rectangular phononic crystals. *Chin. Phys. B* **2019**, *28*, 124301. [CrossRef]
13. Collins, M.J.; Zhang, F.; Bojko, R.; Chrostowski, L.; Rechtsman, M.C. Integrated optical Dirac physics via inversion symmetry breaking. *Phys. Rev. A* **2016**, *94*, 063827. [CrossRef]
14. Xie, X.; Li, H.L.; Peng, Y.G.; Zhu, X.F.; Luo, W.; Zhao, D.G. Switching between deterministic and accidental Dirac degeneracy by rotating scatterers and the multi-channel topological transport of sound. *New J. Phys.* **2019**, *21*, 073047. [CrossRef]
15. Yu, S.Y.; Wang, Q.; Zheng, L.Y.; He, C.; Liu, X.P.; Lu, M.H.; Chen, Y.F. Acoustic phase-reconstruction near the Dirac point of a triangular phononic crystal. *Appl. Phys. Lett.* **2015**, *106*, 151906. [CrossRef]
16. Zhang, Z.W.; Tian, Y.; Cheng, Y.; Liu, X.J.; Christensen, J. Experimental verification of acoustic pseudospin multipoles in a symmetry-broken snowflake like topological insulator. *Phys. Rev. B* **2017**, *96*, 241306. [CrossRef]
17. Huo, S.Y.; Chen, J.J.; Feng, L.Y.; Huang, H.B. Pseudospins and topological edge states for fundamental antisymmetric Lamb modes in snowflakelike phononic crystal slabs. *J. Acoust. Soc. Am.* **2019**, *146*, 729–735. [CrossRef]
18. Jia, D.; Sun, H.X.; Yuan, S.Q.; Zhang, C.; Liu, X.J. Pseudospin-dependent acoustic topological insulator by airborne sonic crystals with a triangular lattice. *Appl. Phys. Express* **2019**, *12*, 044003. [CrossRef]
19. Tian, Z.H.; Shen, C.; Li, J.F.; Reit, E.; Bachman, H.; Socolar, J.E.S.; Cummer, S.; Huang, T.J. Dispersion tuning and route reconfiguration of acoustic waves in valley topological phononic crystals. *Nat. Commun.* **2020**, *11*, 14553. [CrossRef]
20. Gao, H.F.; Zhang, X.; Wu, F.G.; Yao, Y.W.; Li, J. Dirac-like point at the high symmetric M point in a square phononic crystal. *Solid State Commun.* **2016**, *234–235*, 35–39. [CrossRef]
21. Xu, C.Q.; Ma, G.C.; Chen, Z.G.; Luo, J.; Shi, J.J.; Lai, Y.; Wu, Y. Three-dimensional acoustic double-zero-index medium with a fourfold degenerate Dirac-like point. *Phys. Rev. Lett.* **2020**, *124*, 74501. [CrossRef]
22. Jiang, X.; Shi, C.Z.; Li, Z.L.; Wang, S.Q.; Wang, Y.; Yang, S.; Louie, S.G.; Zhang, X. Direct observation of Klein tunneling in phononic crystals. *Science* **2020**, *370*, 1447–1450. [CrossRef]
23. Chen, M.; Xu, W.S.; Liu, Y.; Zhang, M.G.; Pei, D.L.; Jiang, H.; Wang, Y.R. Tunable Dirac cones in two-dimensional acoustic metamaterials with matryoshka structure. *J. Acoust. Soc. Am.* **2019**, *146*, 767–772. [CrossRef]
24. Zhu, Y.L.; Wang, Z.P.; Poh, L.H. Auxetic hexachiral structures with wavy ligaments for large elasto-plastic deformation. *Smart Mater. Struct.* **2018**, *27*, 055001. [CrossRef]
25. Hu, L.L.; Luo, Z.R.; Yin, Q.Y. Negative Poisson's ratio effect of re-entrant anti-trichiral honeycombs under large deformation. *Thin Wall. Struct.* **2019**, *141*, 283–292. [CrossRef]
26. Mousanezhad, D.; Haghpanah, B.; Ghosh, R.; Hamouda, A.M.; Nayeb-Hashemi, H.; Vaziri, A. Elastic properties of chiral, anti-chiral, and hierarchical honeycombs: A simple energy-based approach. *Theor. Appl. Mech. Lett.* **2016**, *6*, 81–96. [CrossRef]
27. Ebrahimi, H.; Mousanezhad, D.; Nayeb-hashemi, H. 3D cellular metamaterials with planar anti-chiral topology. *Mater. Design* **2018**, *145*, 226–231. [CrossRef]
28. Han, X.Z.; Li, L.; Hu, Y.J.; Ling, L.; Geng, Z.G.; Peng, Y.G.; Lu, R.D.; Zhu, X.F.; Wang, X.L. Valley like edge states in chiral phononic crystals with Dirac degeneracies beyond high-symmetry points and boundaries of Brillouin zones. *Phys. Rev. Appl.* **2020**, *14*, 024091. [CrossRef]